JPET Fast Forward. Published on December 17, 2012 as DOI: 10.1124/jpet.112.201400

Pharmacological Inhibition of Mitochondrial Carbonic Anhydrases Protects Mouse Cerebral Pericytes from High Glucose-Induced Oxidative Stress and Apoptosis

Gul N. Shah, Tulin O. Price, William A. Banks, Yoichi Morofuji, Andrej Kovac, Nuran Ercal, Christine M. Sorenson, Eui S. Shin, and Nader Sheibani

Division of Endocrinology, Department of Internal Medicine, Saint Louis University, Edward A. Doisy Research Center, 1100 South Grand Blvd, DRC 354, St. Louis, MO 63104, USA (G.N.S., T.O.P.); VAPSHCS/GRECC S-182, Building 1, Room 810A, 1660 S. Columbian Way, Seattle, WA 98108, USA (W.A.B.); Division of Gerontology and Geriatric Medicine, Department of Medicine, University of Washington, Seattle, WA, USA (W.A.B, Y.M., A.K.); Department of Chemistry, Missouri University of Science & Technology, 400 West 11th Street, Rolla MO 65409, USA (N.E.); and Departments of Pediatrics (C.M.S.) and Ophthalmology & Visual Sciences, University of Wisconsin School of Medicine and Public Health, Madison, WI 53792, USA (E.S.S., N.S.)

Running Title: Mitochondrial CA inhibition protects apoptosis of brain PC

Address correspondence to: Dr Gul N. Shah**,** Division of Endocrinology, Department of Internal Medicine Saint Louis University, Edward A. Doisy Research Center, 1100 South Grand Blvd, DRC 315 St. Louis, MO 63104, Tel.: +1 314 977 9293, Fax: +1 314 977 6797, Email: shahgn@slu.edu

The number of text pages: 33

The number of tables: 1

The number of figures: 6

The number of references: 50

The number of words in abstract: 250

The number of words in introduction: 670

The number of words in discussion: 1102

ABBREVIATIONS: BBB, blood-brain barrier; bFGF, basic fibroblast growth factor; CAs, carbonic anhydrases; CD13, aminopeptidase N; EC, endothelial cells; ETC, electron transport chain; ETZ, 6-Ethoxy-2-benzothiazolesulfonamide (ethoxyzolamide); FACS, fluorescence Activated Cell Sorting; GFAP, glial fibrillary acidic protein; GPI, glycosylphosphatidylinositol; GSH, reduced glutathione; HCO_3^-, bicarbonate; HG, high glucose; HNE, 4-hydroxy-2-trans-nonenal; IFN-γ, interferon gamma; imPC, conditionally immortalized cerebral pericytes; LPS, lipopolysaccharide; mCAs, mitochondrial carbonic anhydrases; NDS, normal donkey serum; NG, normal glucose; NG2, neuron-glial 2; OxSt, oxidative stress; PC, pericytes; PDGFR-β, platelet-derived growth factor receptor β; PDS, plasma derived serum; PECAM-1, platelet

endothelial cell adhesion molecule-1; ROS, reactive oxygen species; α-SMA, smooth muscle actin α-subunit; TEER, transendothelial electric resistance; TCA, trichloroacetic acid; TOP, topiramate; TUNEL, TdT-dUTP Terminal Nick-End Labeling.

Section: Endocrine and Diabetes

JPET Fast Forward. Published on December 17, 2012 as DOI: 10.1124/jpet.112.201400
This article has not been copyedited and formatted. The final version may differ from this version.

ABSTRACT

Diabetes-associated complications in the microvasculature of the brain are caused by oxidative stress, generated by overproduction of reactive oxygen species from hyperglycemia-induced accelerated oxidative metabolism of glucose. Pericytes, essential for the viability of the microvasculature, are especially susceptible to oxidative stress. Mitochondrial carbonic anhydrases, regulators of the oxidative metabolism of glucose, determine the rate of reactive oxygen species production and inhibition of mitochondrial carbonic anhydrases rescues glucose-induced pericyte loss in the diabetic mouse brain. We hypothesized that high glucose induces intracellular oxidative stress and pericyte apoptosis and inhibition of mitochondrial carbonic anhydrases protects pericytes from oxidative stress-induced apoptosis. To validate our hypothesis, conditionally immortalized cerebral pericyte (IPC) cultures were established from immortomice to investigate the effect of high glucose on oxidative stress and pericyte apoptosis. The IPC expressed pericyte markers and induced high transendothelial electrical resistance and low permeability in brain endothelial cell monolayers comparable to pericytes in primary cultures. The IPC also secreted cytokines constitutively and in response to lipopolysacchride similar to pericytes. High glucose caused oxidative stress and apoptosis of these cells with both oxidative stress and apoptosis significantly reduced following mitochondrial carbonic anhydrase inhibition. These results provide the first evidence that pharmacological inhibition of mitochondrial carbonic anhydrases attenuates pericyte apoptosis caused by high glucose-induced oxidative stress. Carbonic anhydrase inhibitors have a long history of safe clinical use and can be immediately evaluated for this new indication in translational research. Thus, mitochondrial carbonic anhydrases may provide a new therapeutic target for oxidative stress related illnesses of the brain.

JPET Fast Forward. Published on December 17, 2012 as DOI: 10.1124/jpet.112.201400
This article has not been copyedited and formatted. The final version may differ from this version.

Introduction

Diabetes mellitus is associated with chronic hyperglycemia, oxidative stress (OxSt) and diabetes-specific microvascular pathology in a variety of tissues including the brain (Giugliano, et al., 1996;Kowluru, 2001;Kowluru, et al., 2004). The microvasculature of the brain comprises the vascular blood-brain barrier (BBB), a regulatory interface that prevents the unrestricted leakage of plasma proteins into the central nervous system and has nutritive, homeostatic, and communication roles. The brain endothelial cells (EC) comprising the BBB are in immediate contact with the pericytes. The pericytes play an important role in the maintenance and homeostasis of the BBB (Dore-Duffy, et al., 2006;Dore-Duffy, 2008) and are especially susceptible to OxSt (Price TO, et al., 2011).

Oxidative stress is caused by overproduction of reactive oxygen species (ROS) primarily during mitochondrial oxidative metabolism of glucose (Du, et al., 2000;Nishikawa, et al., 2000). ROS are produced as byproducts (Chen, et al., 2003;Liu, et al., 2002) of electron transport chain (ETC) reactions during production of ATP as glucose is metabolized to H_2O and CO_2. In diabetes, the hyperglycemic state provides more glucose to the Krebs cycle, especially in insulin-insensitive tissues, thus increasing the rate of production of electron donors, $FADH_2$ and NADH. These electron donors generate a proton gradient across the inner mitochondrial membrane during ETC reactions. When the electrochemical potential difference generated by the proton gradient is high, the lifetime of the superoxide-generating electron-transport intermediates is prolonged (Brownlee, 2001). Beyond a threshold, superoxide production is markedly increased (Korshunov, et al., 1997), thereby causing OxSt. Therefore, a reduction in the rate of production of ROS should reduce OxSt. We recently reported reduction of OxSt in the brain of diabetic-

JPET Fast Forward. Published on December 17, 2012 as DOI: 10.1124/jpet.112.201400
This article has not been copyedited and formatted. The final version may differ from this version.

mice by pharmacological inhibition of mitochondrial carbonic anhydrases (mCA) (Price TO, et al., 2011).

Carbonic anhydrases (CA) catalyze a simple yet fundamental biological reaction, CO_2 hydration to produce bicarbonate (HCO_3^-) and protons (Shah, et al., 2000). This reaction forms the basis for the regulation of acid–base balance in organisms. In addition, CA participate in a number of other physiological processes such as CO_2 and HCO_3^- transport, bone resorption, production of body fluids, gluconeogenesis, ureagenesis and lipogenesis (Sly and Hu, 1995). During evolution, at least 13 active CA isoenzymes have emerged in both rodents and humans. These isozymes have differences in their tissue distribution, kinetic properties and subcellular localizations (Hilvo, et al., 2005). Only two of the known isozymes, designated as CA VA and CA VB, are expressed in the mitochondria (Shah, et al., 2000). These mCA play an important role in the regulation of oxidative metabolism of glucose (Price TO, et al., 2011).

Previously, we reported (Price TO, et al., 2011) rescue of OxSt-induced cerebral pericyte loss in diabetic mice with topiramate, a mCA inhibitor (Nishimori I, et al., 2005). The purpose of the current study was to investigate the mechanism by which high glucose-induced OxSt causes pericyte death and to determine whether inhibition of mCA protects pericytes from OxSt-induced apoptosis. To address these questions, we established conditionally immortalized cerebral pericytes (IPC) from the Immortomouse (Scheef EA, et al., 2009). The IPC can be rapidly expanded under permissive conditions [33˚C in the presence of interferon-gamma (IFN-γ)] and can be readily passaged, frozen, and thawed. We show here that similar to pericytes in primary culture (PC), these cells expressed α-smooth muscle actin (α-SMA), neuron-glial 2 (NG2) proteoglycan, platelet-derived growth factor receptor-β (PDGFR-β), and aminopeptidase N (CD13) markers in both the early and the late passages. In addition, IPC enhanced the

transendothelial electric resistance (TEER) and reduced the permeability coefficient of brain EC monolayers in triple co-cultures (Nakagawa S, et al., 2009) similar to PC. The IPC had an expression pattern for CA's similar to PC: presence of mCA VA and VB, but lack of cytosolic CA II, two transmembrane CA's (CA XII and CA XIV), and lack of the glycosylphosphatidylinositol (GPI)-anchored CA IV.

We now report, for the first time, that high glucose causes intracellular OxSt and pericyte death by apoptosis. We also provide evidence that high glucose-induced intracellular OxSt and pericyte apoptosis are significantly reduced upon pharmacological inhibition of mCA.

Materials and Methods

Animals

Immortomice expressing a temperature-sensitive simian virus (SV) 40 large T antigen and male CD-1 mice were obtained from Charles River Laboratories (Charles River, Wilmington, MA). Male C57BL/6 mice were from Jackson Laboratories (Bar Harbor, ME). All animal experiments were conducted under protocols approved by the Institutional Animal Care and Use Committee.

Preparation of pericytes

Immortalized cerebral pericytes (IPC) were isolated from immortomice back crossed to C57BL/6 mice (Scheef EA, et al., 2009) according to the method of Hayashi et al. (Hayashi, et al., 2004) with modification. Briefly, brains from 5-10 mice (both female and male), ubiquitously expressing a thermolabile strain of tsA58 of the SV40 large T antigen (tsA58 Tag), were removed and placed in DMEM (low glucose; Sigma, St. Louis, MO) on ice. The meninges were removed by gently rolling half of a brain on a sterile filter. The white matter and choroid plexus were removed and the remaining tissue was cut into small pieces and incubated in 25 ml DMEM containing collagenase Type II (1 mg/ml; Worthington, Lakewood, NJ) and DNase I (30 U/ml; Sigma) for 40 min at 37^{o}C. Following incubation, the digest was centrifuged at 500x*g* for 10 min at 4^{o}C. The supernatant was carefully removed by aspiration, the pellet was mixed with 25 ml of 20% BSA prepared in DMEM, mixed well, and centrifuged at 1 000x*g* for 20 min at 4^{o}C. The lipid layer on the top was carefully removed, the pellet which contains the blood vessels was resuspended in 5 ml of collagenase/dispase (1 mg/ml in serum free DMEM containing 0.1% BSA), DNase I (30 U/ml) and incubated at 37^{o}C for 30 min. The digestion was

resuspended by pipetting, centrifuged, and the cell pellet was washed once with 5 ml of DMEM containing 10% FBS. The pellet was resuspended in 1 ml of growth medium consisting of DMEM with 10% FBS, 2mM L-glutamine, penicillin/streptomycin (Sigma) and murine recombinant IFN-γ at 44 U/ml (R&D Systems, Minneapolis, MN), and plated into a well of 24 well plate. The cells were fed every 3-4 days, maintained at 33^{o}C with 5% CO_2, and when confluent expanded to larger tissue culture plates. Because microvessel fragments contain 2-3% pericytes, the pure culture of cerebral pericytes was obtained by prolonged culture of isolated brain microvessel fragments. Pericyte survival and proliferation was favored by selective culture conditions (Kis, et al., 2002). Pericytes were characterized by their large size and rhomboid morphology, positive immunostaining for α-SMA and NG2 (Balabanov and Dore-Duffy, 1998) and the absence of platelet endothelial cell adhesion molecule (PECAM-1) and glial fibrillary acidic protein (GFAP) staining. By flow cytometry, 95% of the cells were positive for both NG2 and α-SMA. Less than 5% of the cells were either positive for NG2 or for α-SMA.

Characterization of IPC

Fluorescence activated cell sorting (FACS) analysis: Mouse IPC were dissociated with Trypsin-EDTA (T3924; Sigma). For immunostaining with anti-mouse PDGFR-β (eBioscience, San Diego, CA) and rat anti-mouse PECAM-1 (Mec13.3, BD Pharmingen), the cells were blocked with 5% FBS in PBS and incubated with an appropriate antibody for 30 min. After washing twice with 5% FBS in PBS, the cells were analyzed by a FACScanCalibur flow cytometer (Becton-Dickinson, Franklin Lakes, NJ). For anti-NG2 (MAB5384, Millipore, Temecula, CA), anti-human α-SMA (MAB1420, R&D systems), and rabbit anti-CD13 (Abcam, MA) immunostaining, dissociated IPC were fixed with 2% paraformaldehyde in PBS for 30 min

and incubated with appropriate primary antibodies in permeabilisation and blocking solution (0.1%BSA and 0.1%Triton X-100 in PBS) for 30 min. Cells were washed and incubated with the appropriate secondary antibody for 30 min, washed, and analyzed by flow cytometry, as described above. All incubations were at 4˚C, all antibodies were used at the dilutions recommended by the supplier. Cells incubated with secondary antibodies only were used as controls.

There are currently no specific markers for pericytes. Staining with α-SMA, PDGFR-β and NG2 is good, but not specific. Therefore, we considered biological functions such as improvement of BBB function and IPC response to lipopolysacchride (LPS) to further characterize these cells (see below).

TEER analysis

Preparation of cells: Mouse brain EC and PC were isolated from 8-week-old male CD-1 mice according to published protocols (Coisne C, et al., 2005;Jacob A., et al., 2010) and (Nakagawa S, et al., 2009), respectively. The glial cells were obtained from neonatal CD-1 mice, by published procedures (Coisne C, et al., 2005;Nakagawa S, et al., 2009). The purity of EC was checked by positive immunostaining for factor VIII (Millipore), zona occludens-1 (ZO-1) (Invitrogen), and claudin-5 (Abcam); of pericytes for α-SMA, CD13, PDGFR-β; and of glial cells for GFAP (Abcam).

Construction of in vitro BBB: The triple culture Transwell model were set up according to published methods (Nakagawa S, et al., 2009). Briefly, glial cells ($1x10^5$ cells/cm^2) were seeded in the wells of Transwell plate and allowed to grow for 3 weeks. PC or IPC ($1.5x10^4$ cells/cm^2) were seeded on the bottom of the collagen-coated polyester membrane (0.33 cm^2, 0.4 μm pore

size) of the Transwell inserts (24-well type, Costar) and allowed to adhere firmly overnight. On the next day, brain EC ($1.5x10^5$ cells/cm^2) were seeded on the inside of the inserts and incubated with glial cell cultures. The BBB models were maintained in an EC medium [DMEM/F12 supplemented with 10% plasma derived serum (PDS, Animal Technologies, Inc., USA), 1% GlutaMAX supplement (Gibco), basic fibroblast growth factor (bFGF, Roche Applied Sciences, 1 ng/ml), heparin (100μg/ml), insulin (5 μg/ml), transferrin (5 μg/ml), sodium selenite (5 ng/ml), and gentamicin (50 μg/ml)] supplemented with 500 nM hydrocortisone at 37°C in a humidified atmosphere of 5% CO_2. TEER (in $\Omega \times cm^2$) was measured using an EVOM resistance meter (World Precision Instruments, Sarasota, FL, USA). The TEER of cell-free Transwell®-Clear inserts were subtracted from the obtained values.

Transendothelial permeability

For the transport experiments, brain EC were washed with physiological buffer (141 mM NaCl, 4.0 mM KCl, 2.8 mM $CaCl_2$, 1.0 mM $MgSO_4$, 1.0 mM NaH_2PO_4, 10 mM HEPES, 10 mM D-glucose and 1% BSA, pH 7.4). The same buffer was added to the outside (abluminal chamber; 0.6 mL) of the Transwell® insert. To initiate the transport experiments, ^{125}I-albumin (5×10^6 cpm/mL) and ^{14}C-sucrose (1.5×10^6 cpm/mL) were loaded on the luminal chamber. Samples (0.5 ml) were removed from the abluminal chamber at 10, 20, 30, and 45 min and immediately replaced with an equal volume of fresh physiological buffer. ^{125}I-Albumin samples were mixed with 30% trichloroacetic acid (TCA; final concentration 15%) and centrifuged at 5 400x*g* for 10 min at 4°C. Radioactivity in the TCA precipitate was determined by a gamma counter, and radioactivity of ^{14}C-sucrose in the collector compartments was measured by a liquid scintillation counter (Tri Carb 1900 from Packard Instrument Company, Perkin-Elmer Life Sciences,

JPET Fast Forward. Published on December 17, 2012 as DOI: 10.1124/jpet.112.201400
This article has not been copyedited and formatted. The final version may differ from this version.

Courtaboeuf, France). The permeability coefficient and clearance of TCA-precipitable ^{125}I-albumin and ^{14}C-sucrose were calculated as described (Dehouck MP, et al., 1992).

Cytokines and chemokines in IPC

The IPC seeded on 24-well culture plate (Costar) were washed with serum-free DMEM/F12, and exposed to culture media with or without LPS from Salmonella typhimurium (L6511; Sigma) at 1 μg/ml for 24 h, as described previously (Kovac, et al., 2011). Culture supernatants were collected and stored at -80^{o}C. The cytokines and chemokines were measured by a commercial magnetic bead Multiple ELISA kit (Bioplex, Biorad, USA) according to the manufacturer's instructions.

Mitochondrial CA VA and CA VB in IPC

Immunoblotting of the whole brain and IPC lysates and RT-PCR of total RNA from the whole brain and IPC was as described previously (Price TO, et al., 2011). Briefly, proteins (50 μg) were separated on 4-12 % Bis-Tris reducing gels (NuPAGE Novex) and transferred to nitrocellulose membranes for immunoblotting. Polypeptides were identified by probing with mitochondrial CA VA and VB primary antibodies (Price TO, et al., 2011) and horseradish peroxidase-conjugated secondary antibodies and visualized by chemiluminescent substrate (Pierce, Rockford, IL). For RT-PCR, RNA (1 μg) was reverse-transcribed with SuperScript III first Strand Synthesis System for RT-PCR (inVitrogen). The double stranded DNA thus produced was used as template for PCR amplification with specific primers for either CA VA or VB as described (Price TO, et al., 2011).

Measurement of OxSt and oxidative damage

The IPC were seeded in 60 mm petri dishes at $5x10^4$ cells/plate. Cells were treated for 5 days with normal glucose (5.7 mM), high glucose (40.7 mM), and high glucose with mCA inhibitors ethoxyzolamide or topiramate at 10 or 100 μM. The cells were dissociated by trypsinization, resuspended in fresh media, and centrifuged. The pellets were analyzed for GSH, a measure of OxSt, and 4-hydroxy-trans-2-nonenal (HNE), a measure of oxidative damage caused by lipid peroxidation. The IPC cultured in L-glucose (D-glucose 5.7mM + L-glucose 35mM) were used for osmolarity control.

To measure GSH, the cell pellets were resuspended in a serine–borate buffer (100 mM Tris–HCl, 10 mM borate, 5 mM serine, 1 mM diethylenetriaminepentaacetic acid, pH 7.0). GSH concentrations were determined by reverse phase HPLC as described earlier (Price TO, et al., 2011).

For lipid peroxidation determination, the cell pellets were resuspended in lysis buffer [0.5% Triton X-100, 20 mM Tris (pH 7.4), 0.15 M NaCl, 2 mM EDTA, 1 mM EGTA, and a protease inhibitor cocktail (#78429, Thermo Scientific)], sonicated, and centrifuged at 14 000x*g* for 15 min: final supernatants were used for detection of HNE by immunoblotting as described earlier (Price TO, et al., 2011).

Measurement of mitochondrial ROS

Mitochondrial ROS in the IPC were measured using MitoSOX^{TM} Red (Invitrogen, USA), a fluorogenic live-cell permeant dye which is chemically and selectively targeted to mitochondria. Once in the mitochondria, MitoSOX is oxidized by superoxide and exhibits red fluorescence (excitation 510 nm/emission 580 nm). The IPC were plated on coverslips at a

density of 2 000 cells/coverslip and allowed to adhere overnight. The cells were then treated with normal glucose (5.7 mM) or normal glucose with or without ethoxyzolamide or topiramate at 100 µM, overnight. After incubation the cells were washed with Hank's balanced salt solution (HBSS, with Ca/Mg) and exposed to normal glucose or high glucose (40.7 mM) for 30 min. At the end of the incubation, cells were washed as before and incubated for 5 min with 2.5 µM MitoSOX, prepared in DMSO immediately prior to the experiment. The cells were thereafter washed with HBSS and counterstained with Hoechst (1:5 000). The digital images were taken by a microscope Olympus BX60 (Tokyo, Japan) with fluorescence equipment. Images were captured using 40x oil immersion objective lens.

Programmed cell death analysis

Apoptotic cell death was determined by TdT-dUTP terminal nick-end labeling (TUNEL) staining. The IPC were grown for 5 days on the fibronectin-coated (2 µg/ml) 4-well Nunc chamber slides (Fisher) under normal glucose, high glucose or high glucose containing 10 or 100 µM of either ethoxyzolamide or topiramate. Following incubation, cells were fixed with 4% paraformaldehyde for 15 min at room temperature and washed with PBS twice. TUNEL staining was performed using Click-iT® TUNEL Alexa Fluor® 594, as recommended by the supplier (Invitrogen). Cells were counterstained with Hoechst for the nuclei and photographed using a Zeiss fluorescence microscope (Axiophot, Zeiss, Germany) equipped with a digital camera. TUNEL-positive cells were counted and calculated as a percentage of the total cell number. The results are from three independent experiments.

Statistical analysis

All means are reported with their *n* and SEM. Two means were compared by the unpaired two-tailed Student's *t* test. For more than two means, ANOVA, followed by Newman-Keuls multiple comparison test, was used. $P<0.05$ was considered significant. Statistical analyses were made using GraphPad Prism 5.0 package program (GraphPad Software Inc, San Diego, CA).

JPET Fast Forward. Published on December 17, 2012 as DOI: 10.1124/jpet.112.201400
This article has not been copyedited and formatted. The final version may differ from this version.

Results

Characterization of IPC

Morphological characterization of IPC: The IPC exhibited the same irregular and stellate morphology as the PC (Fig. 1A). To further assess similarities between IPC and PC, we analyzed IPC for the expression of pericyte markers by FACS analysis. The pericyte markers PDGFR-β (Fig. 1B), α-SMA (Fig. 1C), NG2 (Fig. 1D), and CD13 (Fig. 1E) were all expressed by IPC in both early and late passages. PECAM-1, an EC marker, was not detected in IPC (Fig. 1F).

Physiological relevance of IPC: To ascertain the physiological relevance of IPC, triple culture Transwell BBB models were set up with brain EC, glial cells, and either PC or IPC. Double co-culture BBB models, without pericytes (w/o PC, Fig. 2A) were used as controls. Both PC and IPC (Fig. 2A) caused statistically higher TEER compared to the double co-culture model ($p<0.001$). ^{14}C-Sucrose permeability of brain EC was significantly decreased in the models constructed with either PC or IPC compared to the BBB model w/o PC ($p<0.01$, Fig 2B). A slight decrease in permeability to ^{125}I-albumin (Fig. 2C) observed in the presence of PC or IPC, did not reach statistical significance (Fig. 2C).

LPS stimulated release of cytokines and chemokines by IPC

To further ascertain the functional similarity between PC and the IPC, cytokine and chemokine release in response to LPS treatment was assessed. Ten of twenty-two cytokines and chemokines were secreted constitutively by IPC and sixteen of twenty-two were secreted with stimulation by LPS (Table 1).

JPET Fast Forward. Published on December 17, 2012 as DOI: 10.1124/jpet.112.201400
This article has not been copyedited and formatted. The final version may differ from this version.

Together, these results showed that IPC have morphological and physiological characteristics similar to those of cerebral PC.

Mitochondrial CA in IPC

Previously, we showed by RT-PCR and immunoblotting that cerebral pericytes express mCA (Price TO, et al., 2011). Using the same techniques, we now confirm the expression of both mitochondrial CA VA and VB (Fig. 3) in IPC. Also similar to PC, CA II (a cytosolic), CA XII and CA XIV (two transmembrane), and CA IV (a GPI-anchored) CA were not detected in IPC.

Effect of inhibition of mCA on OxSt in IPC

The cells were incubated under normal glucose (5.7 mM) or high glucose (40.7 mM) conditions for 5 days. Mitochondrial CA inhibitors, ethoxyzolamide or topiramate (10 μM and 100 μM) were added to the high glucose media at the start of the experiment. Compared to normal glucose, high glucose caused significant OxSt in IPC, as is indicated by a decrease in intracellular GSH (Fig. 4A and B). Treatment with ethoxyzolamide significantly increased GSH at 10 μM ($p<0.001$), and at 100 μM ($p<0.0001$), compared to high glucose alone (Fig. 4A). Similarly, topiramate treatment reduced high glucose-induced OxSt (Fig. 4B) by significantly increasing GSH at both 10 μM ($p<0.01$) and 100 μM ($p<0.001$).

Lipid peroxidation, an indicator of oxidative damage, was assessed by the levels of protein-bound HNE, a stable byproduct of lipid peroxidation. The protein-bound HNE levels were significantly increased in IPC exposed to high glucose (Fig 5A and B). The treatment with ethoxyzolamide significantly reduced high glucose-induced protein-bound HNE (Fig. 5A) at

both concentrations used ($p<0.01$ and $p<0.0001$ at 10 μM and 100 μM, respectively). Topiramate treatment significantly reduced high glucose induced protein-bound HNE at 100 μM ($p<0.0001$, Fig. 5C).

Effect of inhibition of mCA on high glucose-induced mitochondrial ROS in IPC

The IPC were grown overnight in normal glucose (5.7 mM) with or without ethoxyzolamide or topiramate and then treated with high glucose (40.7 mM) for 30 min. The cell treated with high glucose showed an increase in mitochondrial ROS as indicated by the intensity of the signal as well as by the number of cells exhibiting the signal (Supplemental Figure 1). Treatment with both ethoxyzolamide and topiramate attenuated high glucose-induced mitochondrial ROS in these cells (Supplemental Figure 1).

Effect of pharmacological inhibition of mCA on high glucose-induced IPC apoptosis

For TUNEL assays, cells were incubated under normal glucose, high glucose, and high glucose with or without mCA inhibitors conditions, as described above. The percent of TUNEL positive IPC grown in normal glucose, high glucose, and high glucose with ethoxyzolamide or with topiramate are shown in Fig. 6A and 6B, respectively. Exposure (5 days) to high glucose caused a significant increase in the percentage of apoptotic cells (Fig. 6A and B) compared to normal glucose. Ethoxyzolamide treatment significantly reduced the number of high glucose-induced apoptotic cells (Fig. 6A) at both concentrations ($p<0.01$). Similarly, topiramate treatment resulted in a significant decrease in the percent of apoptotic IPC ($p<0.0001$) as compared with high glucose (Fig. 6B). Representative TUNEL images of IPC in normal glucose, high glucose, and high glucose with 10 and 100 μM ethoxyzolamide or topiramate are presented in

JPET Fast Forward. Published on December 17, 2012 as DOI: 10.1124/jpet.112.201400
This article has not been copyedited and formatted. The final version may differ from this version.

Supplemental Figure 2. The cells cultured in L-glucose (osmolarity control D-glucose 5.7mM + L-glucose 35mM) for 5 days did not show OxSt or apoptosis.

Discussion

The main findings of this study showed that the pericyte exhibit OxSt and apoptosis responses when exposed to high glucose. Both high glucose-induced OxSt and apoptosis of pericyte were rescued by pharmacological inhibition of mCA.

The pericytes, in immediate contact with the specialized EC of cerebral microvasculature comprising the BBB, are vital for integrity of the latter and are especially susceptible to OxSt. Loss of pericytes results in a focal increase in BBB permeability (Bonkowski, et al., 2011). A close correlation between pericyte density and BBB permeability has been reported in pericyte deficient adult mice (Armulik, et al., 2010). Recently, we reported hyperglycemia-induced OxSt in the brain and cerebral pericyte loss in diabetic mice (Price TO, et al., 2011). Clinical evidence suggests that diabetes-induced changes in the BBB may be a predisposing factor for Alzheimer's disease (Ristow, 2004) and people suffering from both types of diabetes have an increased risk of cognitive impairment (Bruce, et al., 2008;Tiehuis, et al., 2008;Whitmer, 2007). Thus, determining the pathophysiological role of hyperglycemia on pericytes is an important step toward understanding the altered neuronal function and increased susceptibility to cerebrovascular diseases.

Hyperglycemia causes OxSt by generating pathological levels of ROS during accelerated oxidative metabolism of glucose (Du, et al., 2000;Nishikawa, et al., 2000). ROS are produced as a byproduct of oxidative metabolism of glucose and play important physiological functions (Droge, 2002). Following is a brief description of the mechanism of production of ROS in the mitochondria during oxidative metabolism: Glucose is metabolized to pyruvate in the cytosol by glycolysis. Pyruvate enters mitochondria and is carboxylated to oxaloacetate, a key intermediate in the Krebs cycle/ETC pathways. The carboxylation of pyruvate to oxaloacetate requires HCO_3^-.

JPET Fast Forward. Published on December 17, 2012 as DOI: 10.1124/jpet.112.201400
This article has not been copyedited and formatted. The final version may differ from this version.

Since mitochondria are impermeant to HCO_3^- (Dodgson, et al., 1980;Hazen, et al., 1997;Parkkila, et al., 1998) the latter must be produced inside the mitochondria. Mitochondrial CA provide HCO_3^- inside the mitochondria by catalyzing reversible hydration of CO_2 ($CO_2 + H_2O \Leftrightarrow HCO_3^- + H^+$). Pharmacological inhibition of mCA slows down the production of HCO_3^-, limits Krebs cycle/ETC, and thus slows down the production of ROS and subsequent OxSt. Recently we showed that pharmacological inhibition of mCA rescues OxSt-induced pericyte loss in diabetic mouse brain (Price TO, et al., 2011). These findings provide evidence that mCA inhibition may protect BBB from the damage caused by OxSt, thus making mCA a new therapeutic target for OxSt related illnesses of the brain. Pyruvate that builds up in the process is shuttled through anaerobic metabolism (aerobic glycolysis) to produce ATP without producing superoxide. Aerobic glycolysis is not harmful and indeed is preferred by fast growing cells (Vander Heiden, et al., 2009).

To facilitate the determination of the effect of high glucose on intracellular OxSt in pericytes and to investigate a mechanism for pericyte death, we prepared conditionally immortalized pericytes (IPC) cultures from immortomice (Fig. 1A). Unlike PC, the IPC can be readily expanded and manipulated in culture for numerous passages without loss of their characteristics. The immortomouse expresses a thermolabile strain (tsA58) of the SV40 large T antigen (tsA58 Tag) driven by an inducible major histocompatibility complex H-2K promoter, thus eliminating many intrinsic problems with immortalized lines (Lidington, et al., 2002). T antigen expression is functionally evident at the reduced temperature of 33°C and was enhanced in the presence of IFN-γ. Generally, incubation at 37°C in the absence of IFN-γ results in a loss of large T antigen within 48 hours (Lidington, et al., 2002). Recently, Dore-Duffy et al., (Dore-Duffy P, et al., 2011) reported a conditionally immortalized cerebral pericyte cell line established

from immortomice. However, unlike IPC these cells are α-SMA negative and proliferate slowly under permissive conditions (33°C, in the presence of IFN-γ) and are largely quiescent.

The IPC share the morphological (Fig. 1) and physiological (Fig. 2) characteristics of PC. The IPC were also capable of secreting cytokines and chemokines both constitutively and in response to LPS (Table 1), a characteristic similar to that recently reported by us in PC (Kovac, et al., 2011). When grown in high glucose media, IPC showed significant OxSt (Fig. 4 and 5) and apoptosis (Fig. 6). Both high glucose-induced OxSt (Fig. 4 and 5) and apoptosis (Fig. 6) were rescued by the pharmacological inhibition of mCA with either ethoxyzolamide or topiramate.

Previously we used topiramate (Nishimori I, et al., 2005) to reduce OxSt and pericyte loss in vivo in the mouse brain (Price TO, et al., 2011). However, topiramate in addition to its CA inhibitory activity has effects on Na^+-independent Cl-/HCO_3^- channels, sodium channels, and calcium channels (Leniger, et al., 2004). Therefore, in this study we included ethoxyzolamide (Hazen, et al., 1997) which is viewed as a relatively pure CA inhibitor. Use of both of these clinically available drugs increases the assurance that effects found are attributable to CA inhibition. The significant reduction of intracellular OxSt (Fig. 4 and 5), mitochondrial ROS (Supplemental Figure 1) and apoptosis (Fig. 6 and Supplemental Figure 2) of IPC is most likely from the ability of ethoxyzolamide and topiramate to inhibit mCA rather than their discordant mechanisms.

Both ethoxyzolamide and topiramate also inhibit isozymes of carbonic anhydrases other than mCA. Previously, we published that a cytosolic (CA II), two transmembrane (CA XII and CA XIV) and a GPI-anchored (CA IV) carbonic anhydrases are not expressed in cerebral PC (Price TO, et al., 2011). We now report the absence of these same CA isoforms in IPC. Lack of

CA II, CA XII, CA XIV, and CA IV expression in IPC gives credence to our hypothesis that the effects of ethoxyzolamide and topiramate on the reduction of OxSt and apoptosis are due to the inhibition of mCA, amply expressed in IPC (Fig. 3). Studies are under way in our labs to investigate the effect of high glucose on OxSt and apoptosis in cerebral IPC that are null for both mitochondrial CA VA and CA VB.

Topiramate in combination with phentermine has recently been approved for the treatment of obesity. We suggest that an additional benefit of such treatment will be protection from the glucotoxicity of diabetes, such as diabetic retinopathy and other central nervous system manifestation, beyond that accountable from changes in blood glucose levels.

In addition to providing important mechanistic information about diabetic neuropathy, our studies define mCA as a novel molecular pathway that could be targeted in OxSt-related illnesses of the central nervous system. Carbonic anhydrase inhibitors are commercially available, are in clinical use for other conditions, and are relatively well tolerated (Gadde, et al., 2011). The therapeutic use of carbonic anhydrase inhibitors in conditions where glucose-induced OxSt contributes to pathology such as the damage to microvasculature of the brain seen in diabetes mellitus deserves further study.

Acknowledgements

The authors thank Ping Patrick (Saint Louis University) and Xinsheng Zhang (Missouri University of Science and Technology) for their technical assistance and Barbara Harris (Missouri University of Science and Technology) for editorial assistance.

Authorship Contributions

Participated in research design: Shah, Banks, and Sheibani

Conducted experiments: Price, Morofuji, Kovac, and Shin

Contributed new reagents or analytic tools: Sorenson and Sheibani

Performed data analysis: Shah, Price, Morofuji, Kovac, and Shin

Wrote or contributed to the writing of the manuscript: Shah, Price, Banks, Kovac, Ercal, and Sheibani.

Reference List

Armulik A, Genove G, Mae M, Nisancioglu MH, Wallgard E, Niaudet C, He L, Norlin J, Lindblom P, Strittmatter K, Johansson BR and Betsholtz C (2010) Pericytes regulate the blood-brain barrier. *Nature* **468**:557-561.

Balabanov R and Dore-Duffy P (1998) Role of the CNS microvascular pericyte in the blood-brain barrier. *J Neurosci Res* **53**:637-644.

Bonkowski D, Katyshev V, Balabanov RD, Borisov A and Dore-Duffy P (2011) The CNS microvascular pericyte: pericyte-astrocyte crosstalk in the regulation of tissue survival. *Fluids Barriers CNS* **8**:8.

Brownlee M (2001) Biochemistry and molecular cell biology of diabetic complications. *Nature* **414**:813-820.

Bruce DG, Davis WA, Casey GP, Starkstein SE, Clarnette RM, Almeida OP and Davis TM (2008) Predictors of cognitive decline in older individuals with diabetes. *Diabetes Care* **31**:2103-2107.

Chen Q, Vazquez EJ, Moghaddas S, Hoppel CL and Lesnefsky EJ (2003) Production of reactive oxygen species by mitochondria: central role of complex III. *J Biol Chem* **278**:36027-36031.

Coisne C, Dehouck L, Faweeuw C, Delplace Y, Miller F, Landry C, Morissette C, Fenart L, Cecchelli R, Tremblay P and Dehouck B (2005) Mouse syngenic in vitro blood-brain barrier model: a new tool to examine inflammatory events in cerebral endothelium. *Lab Invest* **85**:734-746.

Dehouck MP, Jolliet-Riant P, Bree F, Cecchelli R and Tillement JP (1992) Drug transfer across the blood-brain barrier: correlation between in vitro and in vivo models. *J Neurochem* **58**:1790-1797.

Dodgson SJ, Forster RE, Storey BT and Mela L (1980) Mitochondrial carbonic anhydrase. *Proc Natl Acad Sci U S A* **77**:5562-5566.

Dore-Duffy P, Mehedi A, Wang X, Bradley M, Trotter R and Gow A (2011) Immortalized CNS pericytes are quiescent smooth muscle actin-negative and pluripotent. *Microvasc Res* **82**:18-27.

Dore-Duffy P (2008) Pericytes: pluripotent cells of the blood brain barrier. *Curr Pharm Des* **14**:1581-1593.

Dore-Duffy P, Katychev A, Wang X and Van BE (2006) CNS microvascular pericytes exhibit multipotential stem cell activity. *J Cereb Blood Flow Metab* **26**:613-624.

Droge W (2002) Free radicals in the physiological control of cell function. *Physiol Rev* **82**:47-95.

Du XL, Edelstein D, Rossetti L, Fantus IG, Goldberg H, Ziyadeh F, Wu J and Brownlee M (2000) Hyperglycemia-induced mitochondrial superoxide overproduction activates the hexosamine pathway and induces plasminogen activator inhibitor-1 expression by increasing Sp1 glycosylation. *Proc Natl Acad Sci U S A* **97**:12222-12226.

Gadde KM, Allison DB, Ryan DH, Peterson CA, Troupin B, Schwiers ML and Day WW (2011) Effects of low-dose, controlled-release, phentermine plus topiramate combination on weight and associated comorbidities in overweight and obese adults (CONQUER): a randomised, placebo-controlled, phase 3 trial. *Lancet* **377**:1341-1352.

Giugliano D, Ceriello A and Paolisso G (1996) Oxidative stress and diabetic vascular complications. *Diabetes Care* **19**:257-267.

Hayashi K, Nakao S, Nakaoke R, Nakagawa S, Kitagawa N and Niwa M (2004) Effects of hypoxia on endothelial/pericytic co-culture model of the blood-brain barrier. *Regul Pept* **123**:77-83.

Hazen SA, Waheed A, Sly WS, LaNoue KF and Lynch CJ (1997) Effect of carbonic anhydrase inhibition and acetoacetate on anaplerotic pyruvate carboxylase activity in cultured rat astrocytes. *Dev Neurosci* **19**:162-171.

Hilvo M, Tolvanen M, Clark A, Shen B, Shah GN, Waheed A, Halmi P, Hanninen M, Hamalainen JM, Vihinen M, Sly WS and Parkkila S (2005) Characterization of CA XV, a new GPI-anchored form of carbonic anhydrase. *Biochem J* **392**.

Jacob A., Hack B., Chiang E., Garcia J.G., Quigg R.J. and Alexander J.J. (2010) C5a alters blood-brain barrier integrity in experimental lupus. *FASEB J* **24**:1682-1688.

Kis B, Kaiya H, Nishi R, Deli MA, Abraham CS, Yanagita T, Isse T, Gotoh S, Kobayashi H, Wada A, Niwa M, Kangawa K, Greenwood J, Yamashita H and Ueta Y (2002) Cerebral endothelial cells are a major source of adrenomedullin. *J Neuroendocrinol* **14**:283-293.

Korshunov SS, Skulachev VP and Starkov AA (1997) High protonic potential actuates a mechanism of production of reactive oxygen species in mitochondria. *FEBS Lett* **416**:15-18.

Kovac A, Erickson MA and Banks WA (2011) Brain microvascular pericytes are immunoactive in culture: cytokine, chemokine, nitric oxide, and LRP-1 expression in response to lipopolysaccharide. *J Neuroinflammation* **8**:139.

Kowluru RA (2001) Diabetes-induced elevations in retinal oxidative stress, protein kinase C and nitric oxide are interrelated. *Acta Diabetol* **38**:179-185.

Kowluru RA, Abbas SN and Odenbach S (2004) Reversal of hyperglycemia and diabetic nephropathy: effect of reinstitution of good metabolic control on oxidative stress in the kidney of diabetic rats. *J Diabetes Complications* **18**:282-288.

Leniger T, Thone J and Wiemann M (2004) Topiramate modulates pH of hippocampal CA3 neurons by combined effects on carbonic anhydrase and Cl-/HCO3- exchange. *Br J Pharmacol* **142**:831-842.

Lidington EA, Rao RM, Marelli-Berg FM, Jat PS, Haskard DO and Mason JC (2002) Conditional immortalization of growth factor-responsive cardiac endothelial cells from H-2K(b)-tsA58 mice. *Am J Physiol Cell Physiol* **282**:C67-C74.

Liu Y, Fiskum G and Schubert D (2002) Generation of reactive oxygen species by the mitochondrial electron transport chain. *J Neurochem* **80**:780-787.

Nakagawa S, Deli MA, Kawaguchi H, Shimizudani T, Shimono T, Kittel A, Tanaka K and Niwa M (2009) A new blood-brain barrier model using primary rat brain endothelial cells, pericytes and astrocytes. *Neurochem Int 2009 Mar-Apr;54(3-4):253-63 Epub 2008 Dec 7*.

Nishikawa T, Edelstein D, Du XL, Yamagishi S, Matsumura T, Kaneda Y, Yorek MA, Beebe D, Oates PJ, Hammes HP, Giardino I and Brownlee M (2000) Normalizing mitochondrial superoxide production blocks three pathways of hyperglycaemic damage. *Nature* **404**:787-790.

Nishimori I, Vullo D, Innocenti A, Scozzafava A and Mastrolorenzo A (2005) Carbonic anhydrase inhibitors. The mitochondrial isozyme VB as a new target for sulfonamide and sulfamate inhibitors. *J Med Chem* **48**:7860-7866.

Parkkila AK, Scarim AL, Parkkila S, Waheed A, Corbett JA and Sly WS (1998) Expression of carbonic anhydrase V in pancreatic beta cells suggests role for mitochondrial carbonic anhydrase in insulin secretion. *J Biol Chem* **273**:24620-24623.

Price TO, Eranki V, Banks WA, Ercal N and Shah GN (2011) Topiramate treatment protects blood-brain barrier pericytes from hyperglycemia-induced oxidative damage in diabetic mice. *Endocrinology 2012 Jan;153(1):362-72 Epub 2011 Nov 22* **153**:362-372.

Ristow M (2004) Neurodegenerative disorders associated with diabetes mellitus. *J Mol Med (Berl)* **82**:510-529.

Scheef EA, Sorenson CM and Sheibani N (2009) Attenuation of proliferation and migration of retinal pericytes in the absence of thrombospondin-1. *Am J Physiol Cell Physiol* **296**:C724-C734.

Shah GN, Hewett-Emmett D, Grubb JH, Migas MC, Fleming RE, Waheed A and Sly WS (2000) Mitochondrial carbonic anhydrase CA VB: differences in tissue distribution and pattern of evolution from those of CA VA suggest distinct physiological roles. *Proc Natl Acad Sci U S A* **97**:1677-1682.

Sly WS and Hu PY (1995) Human carbonic anhydrases and carbonic anhydrase deficiencies. *Annu Rev Biochem* **64**:375-401.

Tiehuis AM, van der Graaf Y, Visseren FL, Vincken KL, Biessels GJ, Appelman AP, Kappelle LJ and Mali WP (2008) Diabetes increases atrophy and vascular lesions on brain MRI in patients with symptomatic arterial disease. *Stroke* **39**:1600-1603.

Vander Heiden MG, Cantley LC and Thompson CB (2009) Understanding the Warburg effect: the metabolic requirements of cell proliferation. *Science* **324**:1029-1033.

Whitmer RA (2007) Type 2 diabetes and risk of cognitive impairment and dementia. *Curr Neurol Neurosci Rep* **7**:373-380.

Footnotes

This study was supported by the National Institute of Health [Grants **RO1DK083485** and RC4 EY021357, EY016695, P30-EY016665, and P30 CA014520].

JPET Fast Forward. Published on December 17, 2012 as DOI: 10.1124/jpet.112.201400
This article has not been copyedited and formatted. The final version may differ from this version.

Figure Legends

Figure 1. Characterization of conditionally immortalized cerebral pericytes (IPC). Morphology of IPC cultured on uncoated plates (magnification x10) **(A)**. IPC were stained for PDGFR-β **(B)**, α-SMA **(C)**, NG2 **(D)**, and CD13 **(E)**, all of which were expressed in IPC. PECAM-1 **(F)** an EC marker is not detected in IPC. Histogram data are presented as cell numbers versus log fluorescence intensity of individual cell markers. The controls, shaded histograms, were either cells without antibody **(B** and **F)** or treated with a secondary antibody **(C, D, E)** only. These experiments were performed three times with similar results.

Figure 2. Comparison of TEER and transendothelial permeability of BBB models. The triple models constructed with IPC imposed the same TEER **(A)** and transendothelial permeability **(B** and **c)** as the ones constructed with PC compared to the double models without pericyte (w/o PC). The TEER (expressed as Ω x cm^2) was higher **(A)** and transendothelial permeability coefficient (P_e) [expressed as (cm/minute) x 10^{-3}] was lower for paracellular markers, ^{14}C-sucrose **(B)** and ^{125}I-albumin **(C),** in the presence of either PC or IPC. All data are presented as mean ± SEM (*n*=4). **p<0.01, ***p<0.001.

Figure 3. Mitochondrial CA VA and VB in IPC. Transcripts of CA VA and CA VB in IPC and the brain (**A**). + and – indicate with and without reverse transcriptase, respectively. Polypeptides of CA VA and CAVB in IPC and the brain (**B**).

Figure 4. Effect of pharmacological inhibition of mCA on high glucose-induced GSH levels in IPC. The IPC were exposed to normal glucose (NG, 5.7 mM), high glucose (HG, 40.7 mM), or

high glucose with mCA inhibitors ethoxyzolamide (ETZ) or topiramate (TOP) for 5 days. The GSH levels were measured by HPLC. High glucose-induced significant reduction in GSH levels **(A** and **B)** was restored upon treatment with ETZ **(A)** and TOP **(B)** at both (10 and 100 μM) concentrations of the inhibitors used. The values are expressed as mean ± SEM (*n*=3). *p<0.01, **p<0.001, ***p<0.0001. The graph is representative of three independent experiments.

Figure 5. Effect of pharmacological inhibition of mCA on high glucose-induced lipid peroxidation in IPC. After exposure to normal glucose (NG, 5.7 mM), high glucose (HG, 40.7 mM), or high glucose with mCA inhibitors ethoxyzolamide (ETZ) or topiramate (TOP) for 5 days. The HNE levels in IPC were measured by immunoblotting. High glucose-induced significant increase in HNE **(A** and **C)** was almost completely reversed upon treatment with ETZ **(A)** and TOP **(C)** at both concentrations (10 and 100 μM) of the inhibitors used. **B** and **D** are the representative immunoblots of protein-bound HNE. The values are expressed as mean ± SEM (*n*=3). *p<0.01, **p<0.001, ***p<0.0001. The graph is representative of three independent experiments.

Figure 6. Effect of pharmacological inhibition of mCA on high glucose-induced apoptosis of IPC. The cells plated on chamber slides were treated with normal glucose (NG, 5.7 mM), high glucose (HG, 40.7 mM), or high glucose with 10 and 100 μM of either ethoxyzolamide (ETZ) or topiramate (TOP) for 5 days and stained for TUNEL. A significant increase in TUNEL-positive IPC **(A** and **B)** was reversed by ETZ **(A)** and TOP **(B)** treatment at both concentrations. The nuclei were counterstained with Hoechst. The TUNEL positive cells are presented as a

percentage of total cell numbers. The values are expressed as mean ± SEM (*n*=3). *p<0.01, **p<0.001, ***p<0.0001.

JPET Fast Forward. Published on December 17, 2012 as DOI: 10.1124/jpet.112.201400
This article has not been copyedited and formatted. The final version may differ from this version.

Table 1. Effect of lipopolysaccharide (LPS) on the release of cytokines and chemokines by IPC.

Cytokine/Chemokine	Control (pg/ml)	Treated (pg/ml)
IL-1a	0.26 ± 0.05	0.42 ± 0.03*
IL-1b	N.D.	5.54 ± 0.56
IL-4	0.55 ± 0.06	1.42 ± 0.02**
IL-5	1.66 ± 0.09	2.58 ± 0.11**
IL-6	2.34 ± 0.49	522.55 ± 50.06**
IL-12 (p40)	N.D.	0.73 ± 0.29
IL-12 (p70)	N.D.	5.24 ± 0.70
IL-13	N.D.	20.08 ± 2.30
IL-17	1.47 ± 0.07	2.44 ± 0.14**
GM-CSF	1.12 ± 0.06	22.65 ± 1.64**
KC	306.56 ± 22.91	37631.75 ± 16842.57
MCP-1	3544.39 ± 209.10	11930.87 ± 386.03**
MIP-1a	1.38 ± 0.14	15.50 ± 1.32**
MIP-1b	N.D.	3.04 ± 0.25
RANTES	147.46 ± 13.88	844.01 ± 122.29**
TNF-α	N.D.	5.85 ± 0.09

IPC were exposed to LPS (1 μg/ml) for 24 h. IL; interleukin, GM-CSF; granulocyte-macrophage colony-stimulating factor, KC; keratinocyte-derived chemokine, MCP-1; monocyte-chemo-attractant protein-1, MIP; macrophage inflammatory protein, RANTES; regulated upon activation, normal T-cell expressed, and secreted, TNF-α; tumor necrose factor. Values are mean ± SEM, n = 5. N.D.; not detected. *$p<0.05$, **$p<0.01$ for difference from controls.

Figure 1

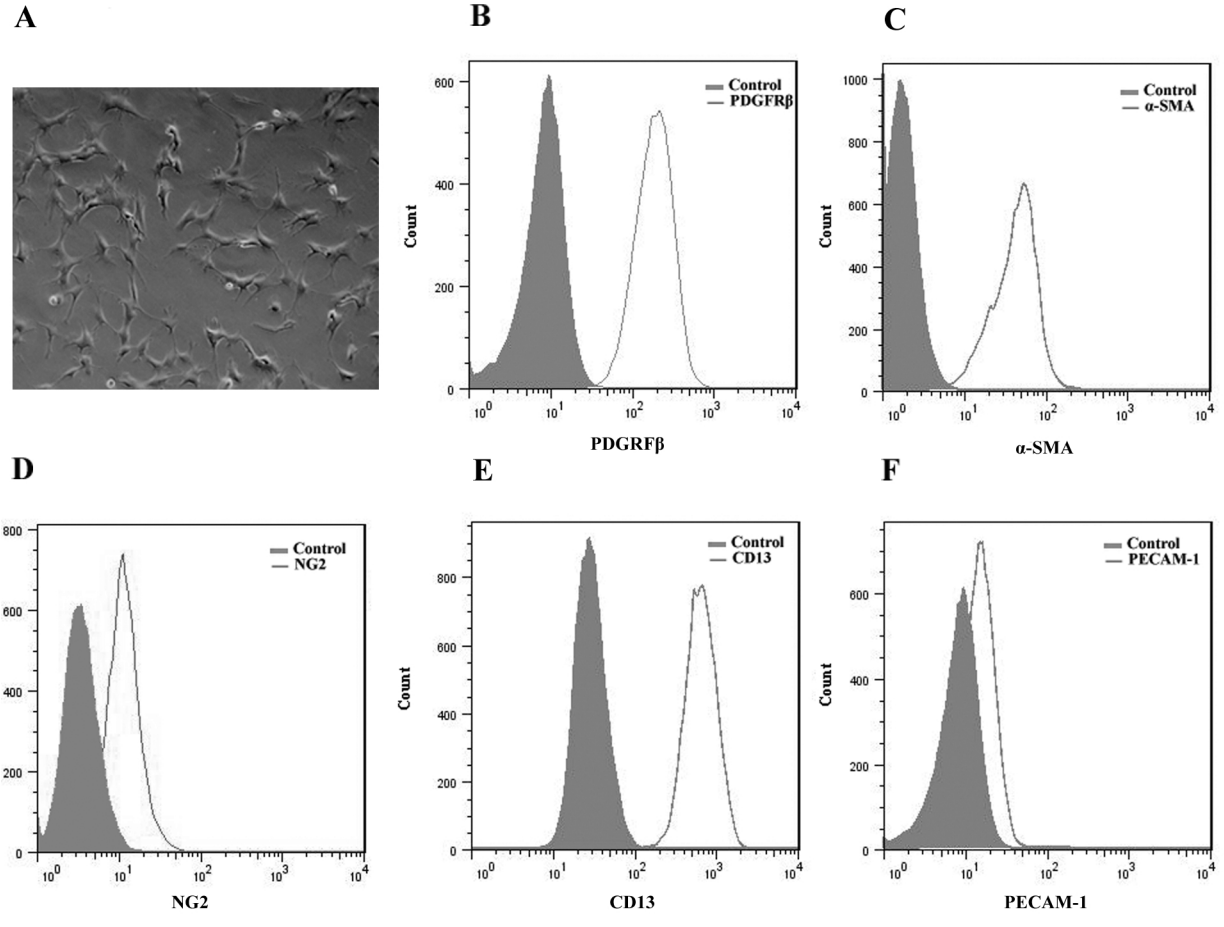
A
B
C
Control
PDGFRβ
Count
PDGRFβ
Control
α-SMA
α-SMA
D
E
F
Control
NG2
NG2
Control
CD13
CD13
Control
PECAM-1
PECAM-1

Figure 2

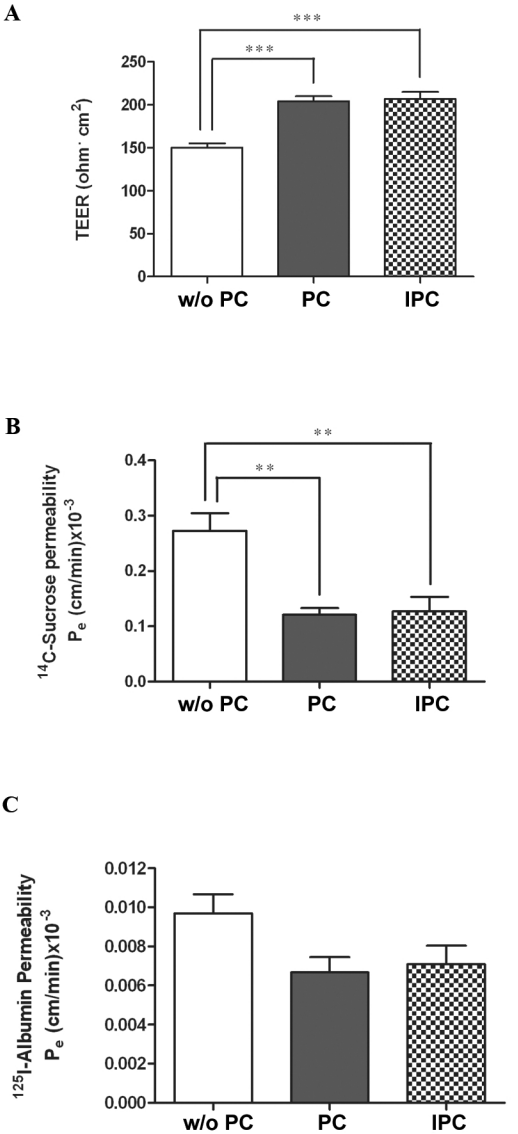
A
TEER (ohm · cm²)
250
200
150
100
50
0
***
***
w/o PC
PC
IPC
B
¹⁴C-Sucrose permeability
Pe (cm/min)x10⁻³
0.4
0.3
0.2
0.1
0.0
**
**
w/o PC
PC
IPC
C
¹²⁵I-Albumin Permeability
Pe (cm/min)x10⁻³
0.012
0.010
0.008
0.006
0.004
0.002
0.000
w/o PC
PC
IPC

Figure 3

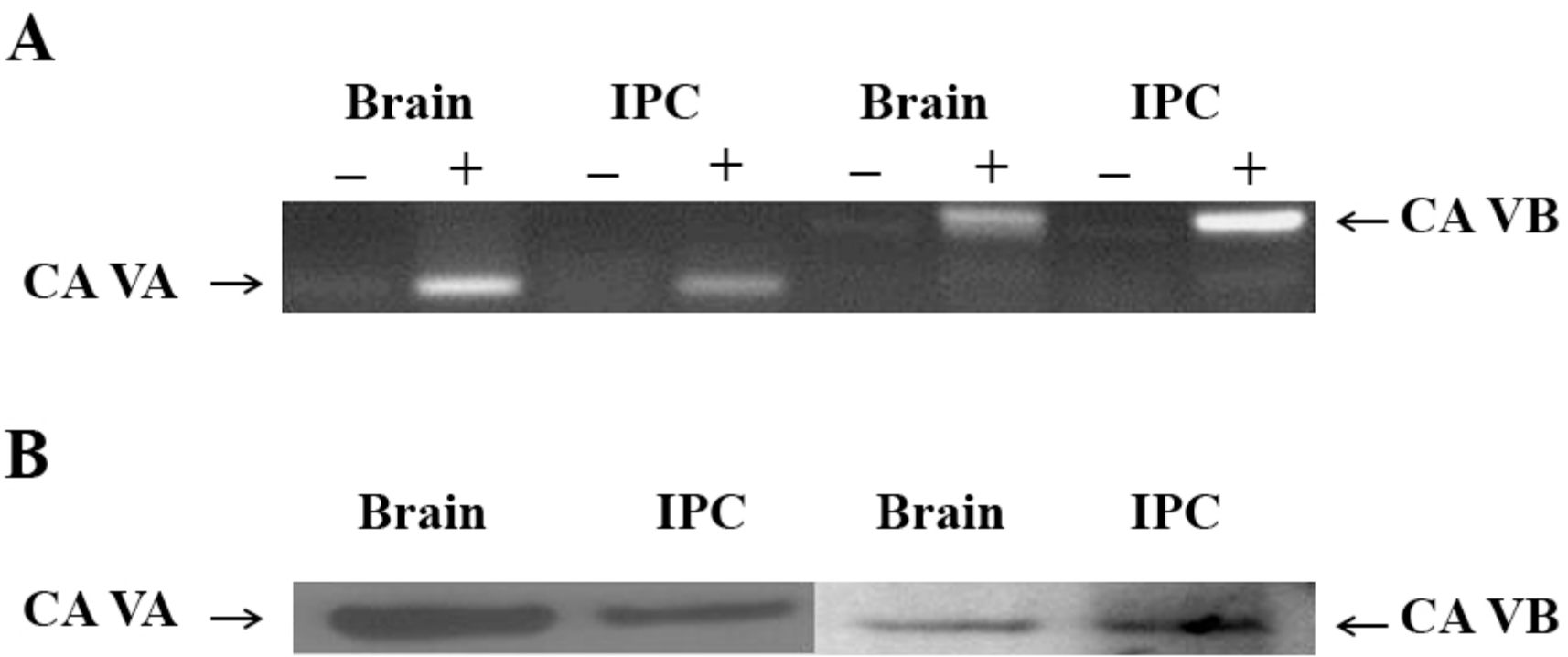
A
Brain
IPC
Brain
IPC
– + – + – + – +
CA VA →
← CA VB
B
Brain
IPC
Brain
IPC
CA VA →
← CA VB

Figure 4

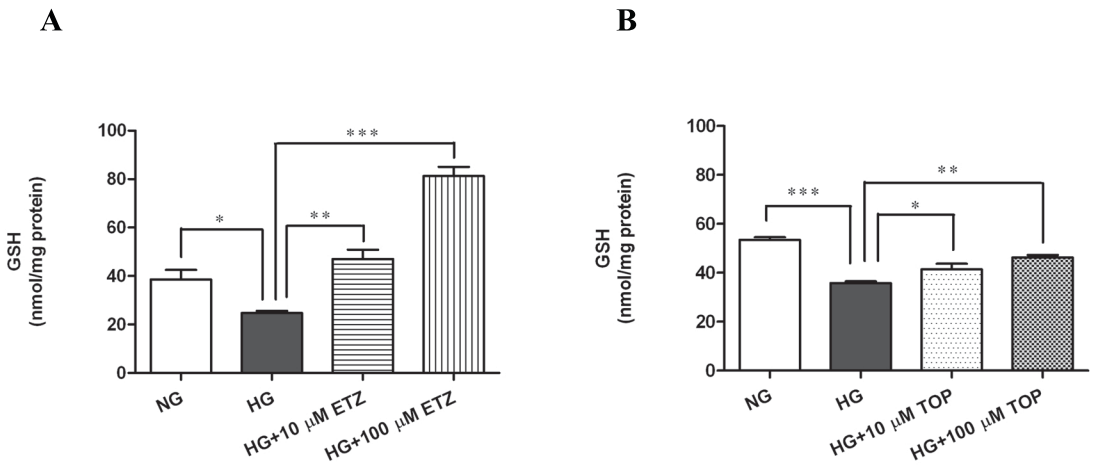
A
GSH (nmol/mg protein)
100
80
60
40
20
0
*
**
***
NG
HG
HG+10 μM ETZ
HG+100 μM ETZ
B
GSH (nmol/mg protein)
100
80
60
40
20
0
***
*
**
NG
HG
HG+10 μM TOP
HG+100 μM TOP

Figure 5

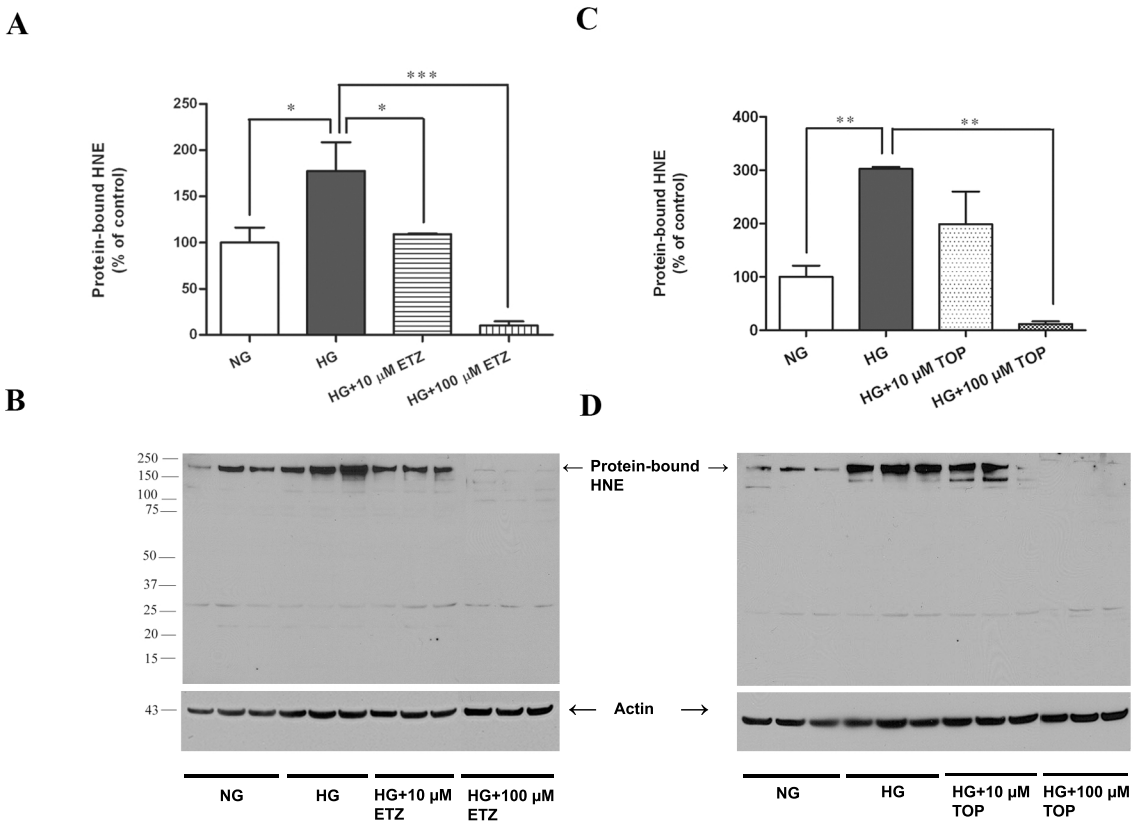
A
Protein-bound HNE (% of control)
250
200
150
100
50
0
*
*
***
NG
HG
HG+10 μM ETZ
HG+100 μM ETZ
C
Protein-bound HNE (% of control)
400
300
200
100
0
**
**
NG
HG
HG+10 μM TOP
HG+100 μM TOP
B
250
150
100
75
50
37
25
20
15
43
← Protein-bound HNE →
← Actin →
NG
HG
HG+10 μM ETZ
HG+100 μM ETZ
D
NG
HG
HG+10 μM TOP
HG+100 μM TOP

Figure 6

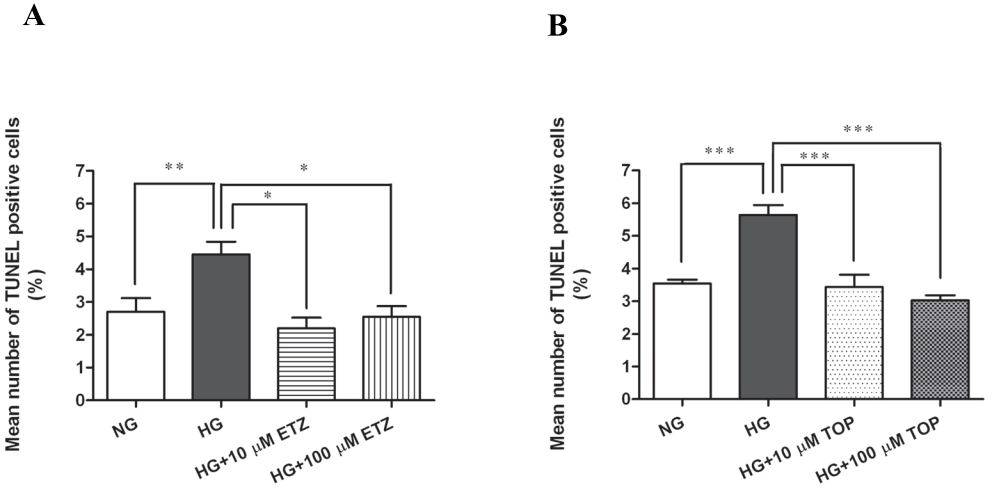
A
Mean number of TUNEL positive cells (%)
0
1
2
3
4
5
6
7
**
*
*
NG
HG
HG+10 μM ETZ
HG+100 μM ETZ
B
Mean number of TUNEL positive cells (%)
0
1
2
3
4
5
6
7
***
***
***
NG
HG
HG+10 μM TOP
HG+100 μM TOP

Pharmacological Inhibition of Mitochondrial Carbonic Anhydrases Protects Mouse Cerebral Pericytes from High Glucose-Induced Oxidative Stress and Apoptosis

Gul N. Shah, Tulin O. Price, William A. Banks, Yoichi Morofuji, Andrej Kovac, Nuran Ercal, Christine M. Sorenson, Eui S. Shin, and Nader Sheibani

Journal of Pharmacology and Experimental Therapeutics
JPET #201400

Supplemental Figure 2

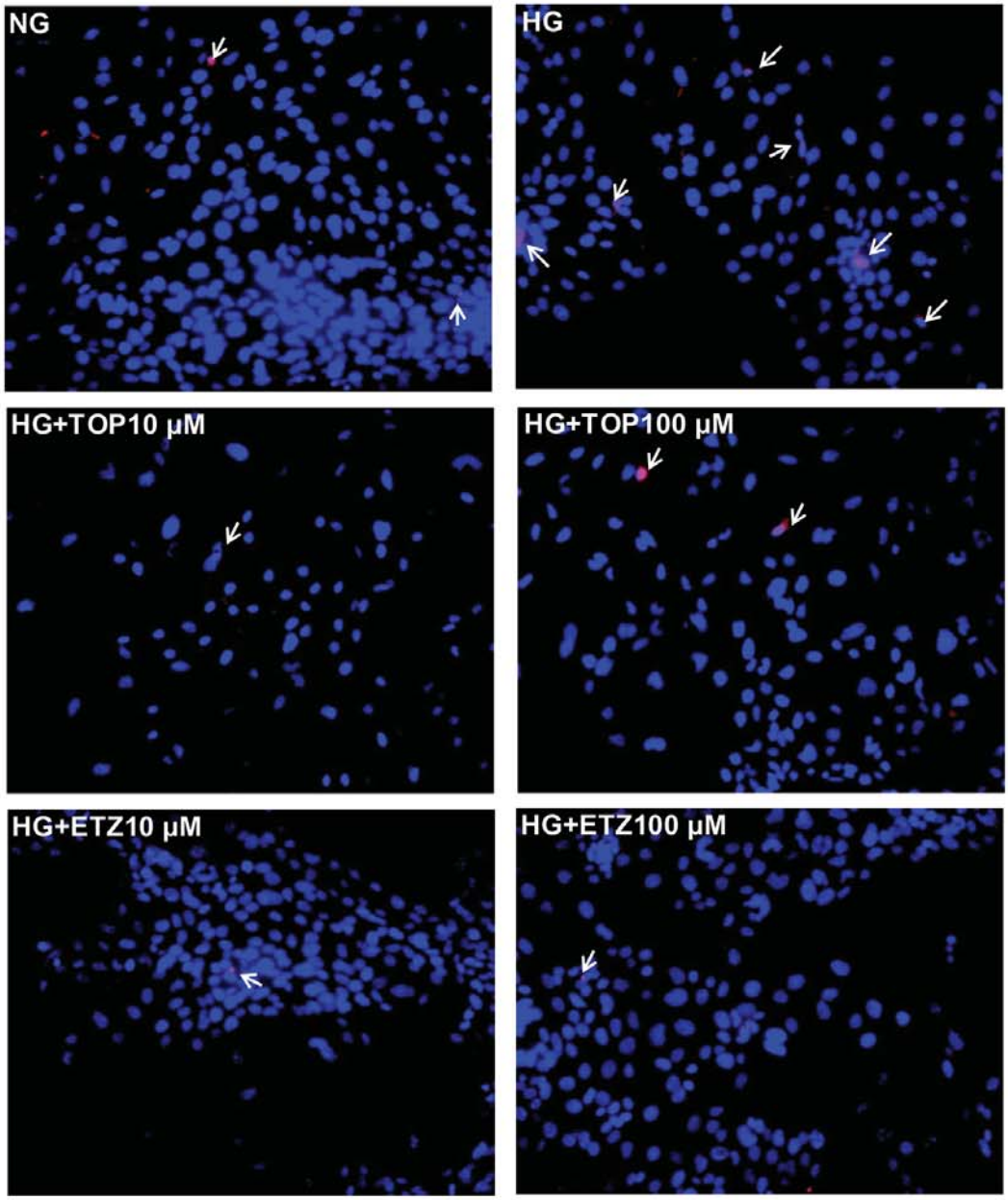

Legend:

TUNEL images showing the effect of inhibition of mCA on high glucose-induced apoptosis in immortalized cerebral pericytes (IPC). The IPC were cultured in normal glucose (NG, 5.7 mM), high glucose (HG, 40.7 mM), or HG with either ethoxyzolamide (ETZ) or topiramate (TOP) for 5 days. Apoptotic cells were discrned by TUNEL staining, nuclei were counterstained with Hoechst. High glucose induced apoptosis was attenuated by both ETZ and TOP at both concentrations (10,100 µM).

Pharmacological Inhibition of Mitochondrial Carbonic Anhydrases Protects Mouse Cerebral Pericytes from High Glucose-Induced Oxidative Stress and Apoptosis

Gul N. Shah, Tulin O. Price, William A. Banks, Yoichi Morofuji, Andrej Kovac, Nuran Ercal, Christine M. Sorenson, Eui S. Shin, and Nader Sheibani

Journal of Pharmacology and Experimental Therapeutics
JPET #201400

Supplemental Figure 1

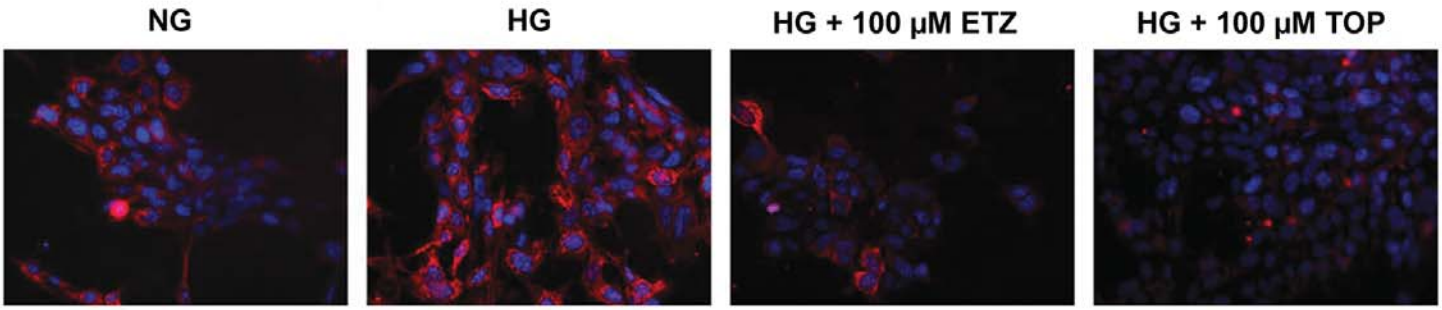

Legend:

Representative fluorescence images showing the effect of inhibition of mCA on high glucose-induced mitochondrial reactive oxygen species (ROS) in immortalized cerebral pericytes (IPC). The IPC were cultured overnight in normal glucose (NG, 5.7 mM) with or without 100 µM ethoxyzolamide (ETZ) or topiramate (TOP). The cells were then exposed to NG or high glucose (HG, 40.7 mM) for 30 minutes and stained with MitoSOX Red. Nuclei were counterstained with Hoechst. High glucose-induced ROS production is attenuated by both ETZ and TOP.